

# The Origin of the Light Distribution in Spiral Galaxies

P. Sánchez-Blázquez<sup>1,2</sup>, S. Courty<sup>1</sup>, B.K. Gibson<sup>1</sup>, and C.B. Brook<sup>1</sup>

<sup>1</sup>*Jeremiah Horrocks Institute for Astrophysics and Supercomputing, University of Central Lancashire, Preston, PR1 2HE, UK*

<sup>2</sup>*Instituto de Astrofísica de Canarias, c/Vía Láctea s/n, E38205, La Laguna, Tenerife, Spain*

Accepted

## ABSTRACT

We analyse a high-resolution, fully cosmological, hydrodynamical disc galaxy simulation, to study the source of the double-exponential light profiles seen in many stellar discs, and the effects of stellar radial migration upon the spatio-temporal evolution of both the disc age and metallicity distributions. We find a “break” in the pure exponential stellar surface brightness profile, and trace its origin to a sharp decrease in the star formation per unit surface area, itself produced by a decrease in the gas volume density due to a warping of the gas disc. Star formation in the disc continues well beyond the break. We find that the break is more pronounced in bluer wavebands. By contrast, we find little or no break in the mass density profile. This is, in part, due to the net radial migration of stars towards the external parts of the disc. Beyond the break radius, we find that  $\sim 60\%$  of the resident stars migrated from the inner disc, while  $\sim 25\%$  formed in situ. Our simulated galaxy also has a minimum in the age profile at the break radius but, in disagreement with some previous studies, migration is not the main mechanism producing this shape. In our simulation, the disc metallicity gradient flattens with time, consistent with an “inside-out” formation scenario. We do not find any difference in the intensity or the position of the break with inclination, suggesting that perhaps the differences found in empirical studies are driven by dust extinction.

**Key words:** galaxies: spiral – galaxies: stellar content – galaxies: kinematic and dynamic – galaxies: structure – galaxies: abundances methods: numerical

## 1 INTRODUCTION

Since 1940, it has been known that the stellar disc light in spiral galaxies decreases exponentially with radius (Patterson 1940; Freeman 1970). This is thought to be the result of the initial angular momentum distribution of the gas cloud that collapsed to form the disc (Fall & Efstathiou 1980; Dalcanton et al. 1997; Mo et al. 1998; van den Bosch 2001; Ferguson & Clarke 2001). However, since the pioneering work of van der Kruit (1979), it has become clear that this exponential profile does not extend to arbitrarily large radii in the majority of disc galaxies. Pohlen & Trujillo (2006) and Erwin et al. (2008) showed – for later and earlier types, respectively – that, in fact, the galaxies for which this happens represent a minority, identifying three classes of surface brightness behaviour in the outskirts of disc galaxies:  $\sim 60\%$  of the galaxies show a deficit of light with respect to an extrapolated singular exponential (Type II);  $\sim 30\%$  show an excess of light in the outskirts respect to a singular exponential (Erwin et al. 2005; Pohlen & Trujillo 2006, Type III); while only  $\sim 10\%$  show pure exponential profiles (Bland-Hawthorn et al. 2005; Pohlen & Trujillo 2006;

Erwin et al. 2008, Type I) out to  $\gtrsim 10$  scale-lengths<sup>1</sup>. Further departure from the notion of the “disc-as-exponential” paradigm leads to even more elaborate classifications based upon, for example, the position of the “break” with respect to the outer Lindblad Resonance of the bar (for Type II) or the exact shape of the surface brightness profile in the outskirts (for Type III) (eg., Pohlen & Trujillo 2006; Erwin et al. 2008).

The break radius ( $R_{\text{br}}$ ), or the radius at which the light profile starts to deviate from a pure exponential is empirically seen to occur at  $\sim 1.5$ – $4.5$  disc scale-lengths (Pohlen & Trujillo 2006). Outside the break, the surface brightness does not immediately drop to zero, but follows a second (different) exponential (de Grijs et al. 2001; Pohlen 2002). The fact that such breaks are very common, at least in late-type galaxies (Beckman et al. 2006), indicates that they either form easily or survive for significant periods of time. The exact causes though, 30 years on from the identification of this “break” phenomenon, remain unclear. The

<sup>1</sup> These percentages are very dependent upon the morphological class of the galaxy (see Beckman et al. 2006).

leading candidates can be divided broadly into those related to angular momentum conservation and those related to a star formation threshold.

In the case of the former, it can be shown that *if* angular momentum redistribution does not occur in the disc, the outermost stellar radius will reflect the maximum value of the angular momentum of the baryonic material (that of the protogalaxy) (van der Kruit 1987). However, numerical simulations have shown that non-axisymmetric instabilities *do* drive a substantial redistribution of angular momentum in the disc (Debattista et al. 2006) and that, in fact, this can be a responsible agent for a break. This is because the angular momentum redistribution leads to an increase in both the central densities and disc scale-lengths. As the angular momentum redistribution cannot act efficiently to arbitrarily large radius, a break in the surface mass density distribution results.

Alternatively, breaks may be due to the effect of star formation thresholds (Kennicutt 1989). Within this latter scenario, the break radius would be located where the density of the gas is lower than the critical value for star formation. The existence of extended UV discs (Thilker et al. 2007; Gil de Paz et al. 2007), the lack of correlation between H $\alpha$  “cutoffs” and optical disc breaks (Pohlen et al. 2004; Elmegreen & Hunter 2006), and the exponential decay of the light outside the break, however, have all been used as arguments against this picture. That said, Elmegreen & Hunter (2006) showed that a double exponential profile *may* result from a multicomponent star formation prescription, where turbulent compression in the outer parts of the disc can allow for cloud formation and star formation despite sub-critical densities. More recently, models have shown that redistribution of stellar material in the disc can also lead to exponential profiles outside the star forming disc’s break radius (Roškar et al. 2008).

Not surprisingly, hybrid models have been suggested which combine aspects of both pictures. For example, van den Bosch (2001) investigated a combination of the collapse and the threshold model, claiming that gas breaks are a direct consequence of the angular momentum of the protogalaxy while the stellar breaks are determined by a star formation threshold.

While each proposed model appears capable of explaining the presence of disc breaks, it is equally important that any successful hypothesis also takes into account the fact that: (i) breaks are not seen in *all* galaxies (Barton & Thompson 1997; Weiner et al. 2001; Bland-Hawthorn et al. 2005); (ii) breaks are seen in discs of *all* morphological types, from S0 (Erwin et al. 2008) to Sm (eg., Kregel et al. 2002; PT06) and even in irregular galaxies (Hunter & Elmegreen 2006) – albeit, not with the same frequency; and (iii) breaks are observed out to redshift  $z \sim 1$  (Pérez 2004; Trujillo & Pohlen 2005; Azzollini et al. 2008b). Recent observational studies have now imposed additional constraints on the models for break formation. For example, de Jong et al. (2007) have shown that the break position is independent of stellar age, a result compatible with that of Bakos et al. (2008), who found the position of the break to be independent of the photometric band. It has also been found that the prominence or intensity of the break decreases with increasing distance from the galactic mid-

plane (de Jong et al. 2007) and for older stellar populations (Bakos et al. 2008; Azzollini et al. 2008a).

Furthermore, the recent work of Roškar et al. (2008) has demonstrated the importance of stellar migrations in defining the final mass density and surface-brightness density profiles of disc galaxies. The re-organization of stars in the disc can have important consequences for the observational constraints used for the chemical evolution models, as the age-metallicity relation or the metallicity distribution, as previously shown by several studies (e.g. Haywood 2006, 2008; Schoenrich & Binney 2008; Roškar et al. 2008).

Previous work in this area has concentrated upon somewhat idealised scenarios of isolated galaxies. The advantage of this approach is that higher resolution can be achieved more readily, with a greater associated exploration of parameter space. However, such an approach necessarily carries with it the disadvantage of not being able to take into account various processes such as the cosmological infall of gas and/or the interactions with other galaxies that are intrinsic to the hierarchical assembly paradigm. Indeed, interactions with satellites can have an important influence in shaping the disc, as suggested by simulations (e.g., Younger et al. 2007; Peñarrubia et al. 2006) and should not be ignored. Our work aims to fill this hole by addressing the possible physical origins of the two-component surface brightness profiles, but now within a cosmological context. We will examine the likelihood that such profiles are the consequence of dynamical processes, star formation processes, or a combination of the two.

## 2 SIMULATION DETAILS

Our simulated disc was realised using multi-resolved, cosmological simulations generated with the N-body, hydrodynamical code RAMSES (Teyssier 2002) which is based upon an Adaptive Mesh Refinement (AMR) technique. RAMSES includes gravitation, hydrodynamics, radiative cooling, and heating processes, immersed within a uniform, Haardt & Madau (1996) ionising radiation field. In addition to solving the Euler equations with a net cooling term, RAMSES includes a phenomenological treatment of star formation, which contributes directly to the chemical enrichment of the interstellar and intergalactic medium via subsequent Type II supernovae.<sup>2</sup> The spatio-temporal evolution of the gas metal abundance, as well as the redshift-dependent photoionising background, are consistently accounted for in the computation of the net cooling rates of the gas (Courty & Teyssier 2009, in preparation). This combined contribution has been fit using the CLOUDY photoionisation code (Ferland et al. 1998).

The star formation prescription within RAMSES is described in detail by Dubois & Teyssier (2008); only a brief summary is provided in what follows. Star formation is permitted in cells whose density is higher than a given thresh-

<sup>2</sup> The current implementation of chemistry within RAMSES is restricted to the global metal content ( $Z$ ), under the assumption of the instantaneous recycling approximation; an extension to RAMSES which relaxes this approximation and includes the effects of Type Ia supernovae and asymptotic giant branch stars is currently under development (Few et al. 2010, in preparation).

old, according to the following rate:  $\dot{\rho}_* = -\rho/t_*$ , where the star formation timescale is proportional to the local free-fall time,  $t_* = t_0(\rho/\rho_0)^{1/2}$ . As in Dubois & Teyssier’s work, we set this timescale to  $t_0 = 8$  Gyr, with an associated density threshold for star formation of  $\rho_0 = 0.1 \text{ H cm}^{-3}$ . Kinetic feedback of supernovae energy to the surrounding interstellar medium is modeled with a blast-wave solution that essentially mimics the expansion of superbubbles whose radius is fixed to two cells. Thermal feedback is accounted for by using a polytropic equation of state in the high-density regions. The amount of gas then turned into stellar material in each eligible gas cell is  $m_*(1 + \eta_{SN} + \eta_W)$ , where the mass locked in long-lived stars is  $m_*$ , and  $m_*(\eta_{SN} + \eta_W)$  is the mass carried away by the blast-wave, with the wind driving parameter  $\eta_W = 1$ , and the mass fraction of stars recycled into supernovae ejecta  $\eta_{SN} = 0.1$ . Photometric properties of the resulting stellar populations were derived by assuming that each star particle was a single stellar population (SSP), and then applying the models of Bruzual & Charlot (2003) with a Salpeter (1955) initial mass function (IMF) and the Bertelli et al. (1994) isochrones.

We run our simulation to  $z = 0$  in a  $\Lambda$ CDM Universe with the following cosmological parameters,  $\Omega_\Lambda=0.7$ ,  $\Omega_m = 0.3$ ,  $\Omega_b=0.045$ ,  $\sigma_8=0.9$  and  $H_0 = 73 \text{ kms}^{-1}\text{s}^{-1}\text{Mpc}^{-1}$ . To carry out cosmological simulations of disc galaxies at the sub-kpc scale, a multi-resolved approach was adopted. Candidate dark matter halos were chosen in a low-resolution, large-scale structure simulation. The size of this  $\Lambda$ CDM simulation was  $20h^{-1} \text{ Mpc}$ , contains  $128^3$  dark matter particles, and was generated with RAMSES as part of the Horizon Project<sup>3</sup>. Our multi-resolved simulation used three nested boxes whose initial conditions were centred on our candidate halo and whose resolution ranged from  $128^3$  in the external part of the computational volume to  $512^3$  for the most nested box. The latter resolution is also the one of the coarse grid in the central area and the adaptive mesh nature of RAMSES was employed to refine a further seven levels, thereby reaching a spatial resolution of 435 pc in the central area by  $z=0$ . Dark matter particles have a mass of  $6 \times 10^6 M_\odot$  and the initial gas mass per cell was  $\sim 10^6 M_\odot$ .

As noted in Gibson et al. (2008), the selection of the candidate halo was made without any preconceptions regarding spin  $\lambda$  or triaxiality  $T$ . Care was taken though to ensure that the final halo was not contaminated by low-resolution dark matter particles up to at least five virial radii. The disc galaxy discussed here sits within a low-spin ( $\lambda=0.02$ ), mildly oblate triaxial ( $T=0.32$ ) halo of dynamical mass  $7.6 \times 10^{11} M_\odot$ . For redshifts  $z < 2.3$ , the rotational axis of the disc could be aligned readily using the angular momentum vector of the gas cells; the analysis which follows is therefore restricted to  $z < 2.3$ . Further technical details of the simulation and alignment process are forthcoming (Courty et al. 2009, in preparation).

### 3 CHARACTERISTICS OF THE DISC

Hydrodynamical simulations of galaxies within the canonical hierarchical structure assembly framework are known to

have a number of difficulties in reproducing disc-dominated galaxies (e.g., Springel & Hernquist 2003; Abadi et al. 2003; Bailin et al. 2005; Okamoto et al 2005; Governato et al. 2007; Scannapieco et al. 2008a). A major problem is that baryons condense early and then transfer a significant fraction of their angular momentum to the dark matter as the final galaxy assembles (Navarro & White 1994). As a result, these galaxies contain a significant fraction of their final baryonic mass in a spheroidal-like component supported primarily by velocity anisotropy, with consequent bulge-to-disc ratios in excess of those encountered in late-type spirals today.

To derive the bulge-to-disc ratio of our simulated galaxy, we categorise the stars as “disc” or “spheroid” following Abadi et al. (2003b) and Scannapieco et al. (2008). We derive the distribution of the circularity parameter  $\epsilon$  (where  $\epsilon = j_z/j_{\text{cir}}$ , and  $j_z$  is the  $z$ -component of the specific angular momentum of each star, where the  $z$ -axis is the symmetry axis and  $j_{\text{cir}}$  is the angular momentum expected for a circular orbit at the same radius,  $r$  – i.e.,  $j_{\text{cir}} = rv_{\text{cir}}(r)$ ). Figure 2 shows the  $\epsilon$  distribution of all stellar particles within a sphere of radius of 20 kpc at  $z=0$  (black). We have marked, with different colours, those particles inside a sphere of radius 1.5 kpc (red), and those with radius  $3 < r < 15$  kpc and within 3 kpc of the disc mid-plane (green). Considering a stellar disc composed of stars with  $r < 15$  kpc,  $|z| < 3$  kpc, and  $0.8 < \epsilon < 1.2$ , and including only those stars rotating in the plane of the disc (with  $\cos \alpha > 0.7$ , where  $\alpha$  is the angle between the angular momentum vector of the particle and the  $z$ -axis, after Scannapieco et al. 2008b), the disc-to-total ratio in our galaxy – measured as the ratio between the stellar mass on the disc and the total stellar mass – is 0.37. Put another way, the bulge-to-disc ratio is, not surprisingly (and in keeping with the aforementioned particle-based disc simulations), large with respect to that observed in late-type spirals (Sb-Sd), being more consistent with the ratio expected for an early-type (Sa-S0) galaxy. Figure 1 shows a bulge-to-disc decomposition of our simulation, using the K-band light profile and employing an exponential law for the disc and a Sersic law for the bulge. The fit was done in an iterative manner, following MacArthur et al. (2003), resulting in a photometric bulge-to-disc ratio of  $\log(B/D) = -0.5$ , consistent with that expected for an early-type (Sa-S0) galaxy (e.g. morphological type T $\sim$ 3: Simien & de Vaucouleurs 1986).

The stellar bulge associated with our simulated disc is partially supported by rotation (with  $V_{\text{rot}}/\sigma \approx 0.5$ , where  $V_{\text{rot}}$  is the maximum rotational velocity). In the simulation here, much as for the Milky Way bulge (admittedly, perhaps just coincidentally),  $V_{\text{rot}} = 70 \text{ km s}^{-1}$ .

Figure 3 shows a density map of the stellar disc from two different perspectives (face-on and edge-on). The disc extends to  $\sim 20$  kpc, with an exponential scale-length (measured in the V-band) of  $\sim 3.2$  kpc, consistent with values found for late-type spirals such as the Milky Way (e.g. Jurić et al. 2008 suggest a scale-length for the Milky Way’s disc of  $\sim 2.6$  kpc).

While the stellar disc extends to  $\sim 20$  kpc, the bulk of our analysis is restricted to stars within a radius of 15 kpc. This is mainly due to the “law-of-diminishing-returns” in the outskirts where the number density of stellar particles decreases dramatically and the root-mean-square (RMS) dispersion of relevant azimuthally-averaged quantities begins

<sup>3</sup> <http://www.projet-horizon.fr>

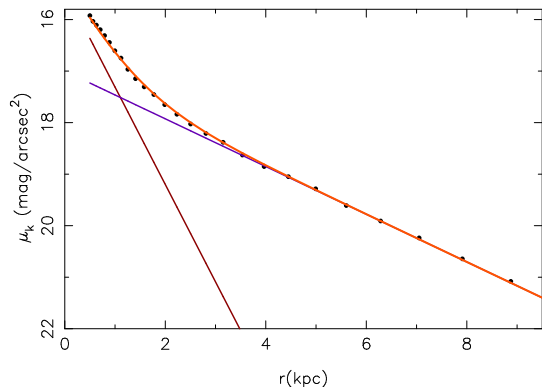


**Figure 1.** K-band surface brightness profile of our simulated disc, plotted out to  $\sim 3$  disc scalelengths. The fitted profiles of the disc (exponential law, shown in purple) and the bulge (Sersic law, shown in dark red) are overlaid, along with the sum of the two (shown in orange).

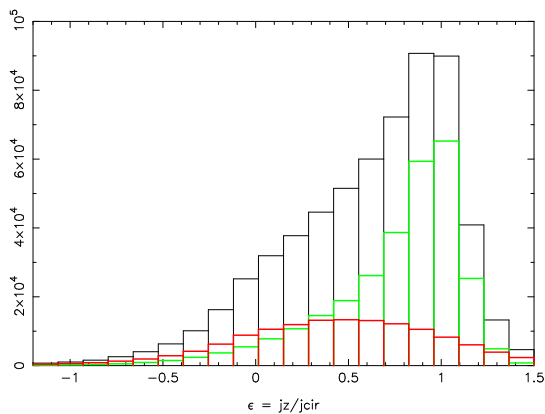


**Figure 2.** Distribution of  $\epsilon = j_z / j_{\text{cir}}$  for all stars within a sphere of  $r < 20$  kpc (black line), within a sphere of 1.5 kpc (red line), and all those with  $3 < r < 15$  kpc and distance from the mid-plane  $< |z| < 3$  kpc (green line).

to increase rapidly. Furthermore, considering only particles inside this 15 kpc radius means we also reduce the possible contamination from co-spatial stellar halo particles.

We end by noting that all “error bars” plotted throughout the paper are derived from the RMS associated with the mean values from eight arbitrary octants of the disc.

#### 4 CHARACTERISTICS OF THE DISC BREAK

The first two rows of Figure 4 show the evolution of the azimuthally-averaged surface brightness profile in the V-band and the total stellar surface density profile, respectively, at five different epochs from  $z=2$  to  $z=0$ . It can be seen that the disc has already developed a break by  $z \sim 1$  in the surface brightness profile and maintained its presence through to  $z=0$ . We fit simple functional forms ( $\mu(R) = \mu_0 + 1.086 \times R/h$ ) to the inner and outer exponentials and consider that the break occurs at the position where the functions intersect. At redshift  $z = 0$ , the break radius is  $R_{\text{br}} \approx 9.5$  kpc (i.e.,  $\sim 2.9$  disc scale-lengths). The break intensity – measured as the angle between the inner and outer exponential profiles – changes with redshift, but

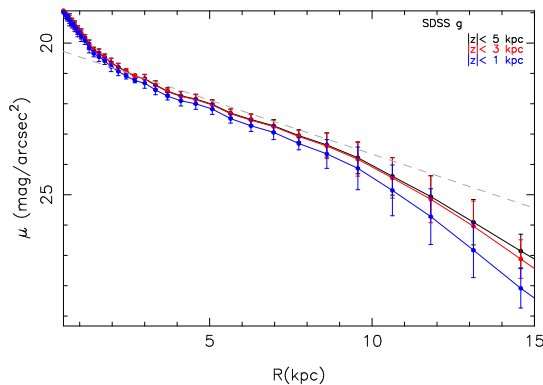


**Figure 6.** Azimuthally-averaged surface brightness profiles in the SDSS g-band, integrating particles within 1, 3, and 5 kpc from the mid-plane, as indicated in the inset. Error bars represent the RMS dispersion between the mean values found in eight arbitrary octants of the disc.

not in any obvious monotonic/systematic manner. It can also be seen that the break is much shallower in the total stellar mass surface density distribution. In fact, in most snapshots it is almost non-existent, a point to which we return in Section 7.1.

Figure 5 shows spatially-resolved 2-dimensional star formation rate (SFR) maps of our simulation at  $z=0$ . The break radius is denoted by the vertical arrows (edge-on view) and circle (face-on view); an immediate point of interest is that there remains measurable star formation outside the break radius. This star formation is not axisymmetric, with star formation extending beyond  $R_{\text{br}}$  on one side, in particular. Such star formation in the outer disc (beyond the break radius) has been observed in many galaxies (Ferguson 1998; Ferguson et al. 1998; Thilker et al. 2005, 2007; Gil de Paz et al. 2007). Before assessing the physical origins driving the formation of the break in the surface brightness profile, we first review the main observational characteristics, to determine if our light profile is a fair representation of those observed in real galaxies.

##### 4.1 Dependence of the break upon distance from the mid-plane

In the case of NGC 4244, de Jong et al. (2007) show that the break occurs at the same radius independent of height above the mid-plane. They further demonstrate that the intensity of the break decreases with height above the plane. Figure 6 shows the surface brightness profiles derived from our simulation, in the SDSS g-band, for samples of stellar particles at different distances from the plane. The empirical characteristics seen by de Jong et al. (2007) are similarly seen in the simulation – specifically, the break radius position does not change with distance from the mid-plane, but it gets shallower.

##### 4.2 Dependence of the profile upon photometric band

Different photometric bands are sensitive to different stellar populations. While the main contributors to the luminosity

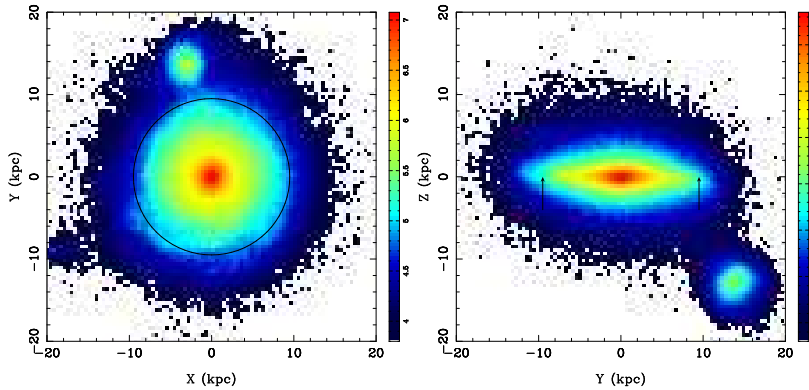


**Figure 3.** Stellar density projections of the disc (left: face-on; right: edge-on). A  $40 \times 40 \times$  kpc region is shown in both panels. The circle in the left panel and the arrows in the right panel indicate the position of the break radius (see Sec. 4).

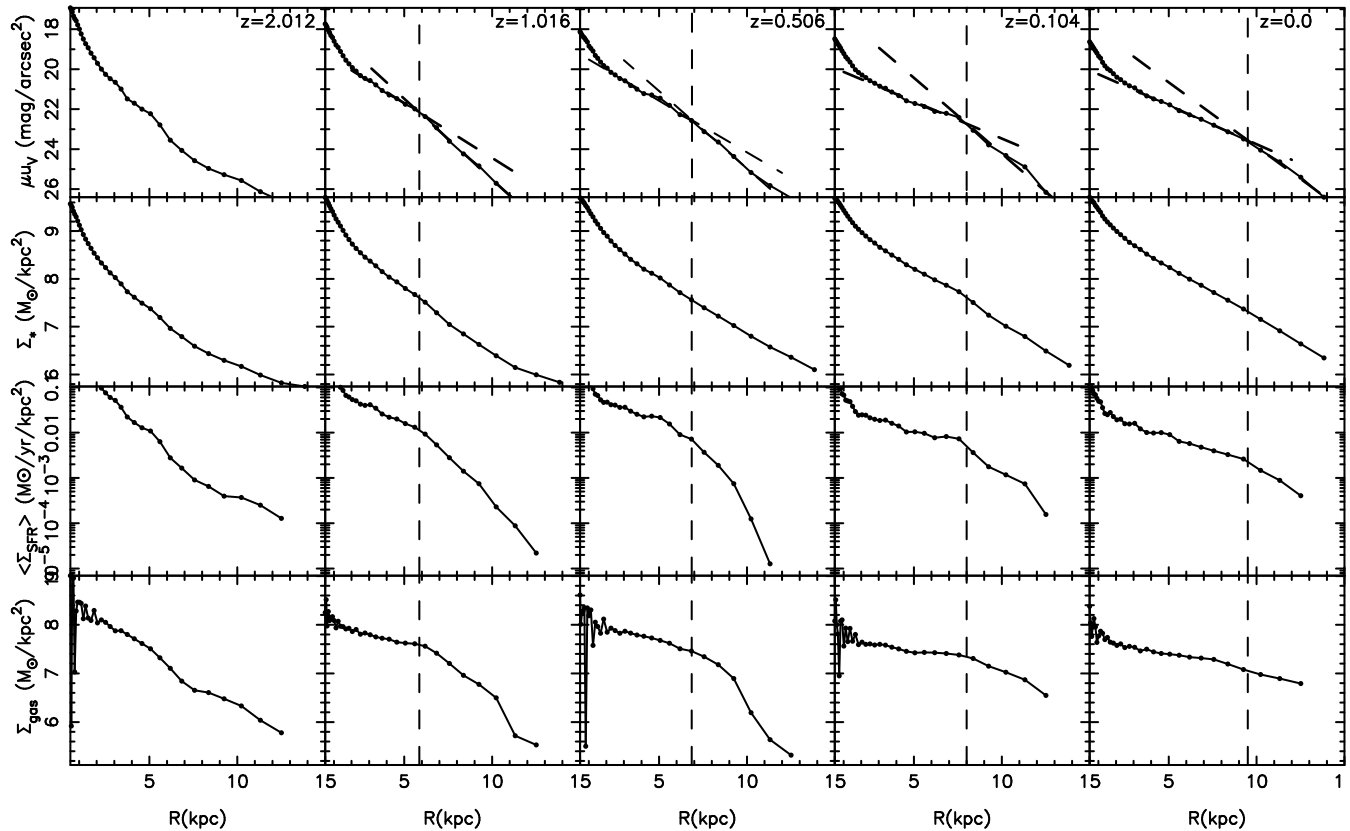


**Figure 4.** Evolution with redshift – as indicated in the inset to each panel – of the V-band surface brightness profile (first row), total stellar surface density profile (second row), star formation rate surface density profile (third row), and gas surface density profile (fourth row), all on logarithmic scales. The profiles were derived using all stars with  $r < 15$  kpc and  $|z| < 3$  kpc. Dashed lines represent fits to the inner and outer exponentials in the V-band surface brightness profile. The break radii correspond to the intersection point of these two exponentials, and are noted by the vertical dashed lines in each panel.

in the blue bands are the young stars,<sup>4</sup> this contribution decreases for the redder bands. Interestingly, Bakos et al. (2008) have found recently that the position of the break is independent of the photometric bandpass employed to

obtain the surface brightness profile, although break is shallower in the redder bandpasses. These results suggest that the break is due mainly to a truncation in the profile of the young stars and that the profile of the old stars should not show the same departure from a pure exponential.

<sup>4</sup> Other hot stellar populations, including blue horizontal branch stars and blue stragglers, may provide an additional contribution in some systems (see, e.g., Rose et al. 1985; Maraston & Thomas 2000; Trager et al. 2005)

Figure 7 shows the surface brightness profiles of the stellar disc in the same two photometric bands (g and r) used in the empirical study of Bakos et al. (2008), in addition to the redder K-band. In our simulation, the break appears at the

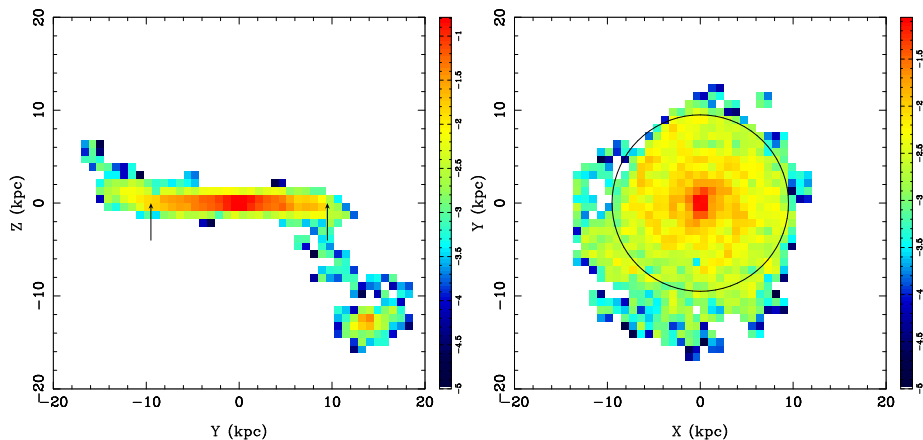


**Figure 5.** Edge-on and face-on 2-dimensional projections of the present-day integrated (over the last 100 Myr) SFR for our cosmological disc. For the face-on projection, only the stars at a distance of 5 kpc from the plane are included, to avoid contamination from the companion. The total line-of-sight in the edge-on projection is 40 kpc. The vertical arrows (edge-on) and circle (face-on) correspond to the position of the break radius in the V-band surface brightness distribution.

same position ( $\sim 9.5$  kpc) but, in agreement with the observations, is also shallower in the redder band (Ks) than it is in the bluer one (g). Furthermore, Bakos et al. (2008) transform the surface brightness profiles into total stellar mass density profiles, using mass-to-light ratios inferred from the colours, following the prescriptions of Bell et al. (2003). This process is admittedly not free of uncertainties, but, at face value, their results suggest that the mass density profile does not show a break, in agreement with that found for our simulated disc (see Fig. 4).

Figure 8 shows the stellar mass surface density distribution in our simulated disc for stars of different ages. While the position of the break is the same for those stellar populations showing a break in the stellar density distribution, not all stars show this truncated density profile. In particular, stars older than  $\sim 8$  Gyr show, if anything, a slightly “upbending” profile. This latter result agrees with a number of observational studies: Davidge (2003) studied the stellar populations in the outskirts of NGC 2403 and M33, showing that while the number of young main-sequence stars present a “downbend” with radius, the number density of the more evolved stars in the red- and asymptotic-giant branch phases do not; Similar results were also obtained by Galleti et al. (2004) for M33. Conversely, for the case of NGC 4244, de Jong et al. (2007) claim a sharp break even when only red giant stars (old stars for a constant star formation history) are considered. This issue clearly needs resolving with a larger sample of galaxies.

### 4.3 Colour profiles

Recently, Bakos et al. (2008), for the local universe, and Azzollini et al. (2008b), out to redshift  $z \sim 1.1$  (see also Jansen et al. (2000)) have found that the colour gradients of galaxies with Type-II truncations are different from those with Type-I or pure exponential profiles (recalling the nomenclature introduced in Section 1). In particular, galaxies showing Type-II truncations have a “U-shaped” colour profile, with the minimum (bluest color) at the position of the break.

Figure 9 shows our predicted colour profile at four dif-

ferent epochs from  $z=1$  to  $z=0$ . In agreement with the observations, our simulated disc also shows a U-shaped profile with the bluest colours near the position of the break.

### 4.4 Age and metallicity profiles

Colours are difficult to interpret in terms of simple stellar populations due to the well-known “age-metallicity degeneracy” (Worthey 1994); in principle, the colour profile could be an effect of age, metallicity, or a combination of both. Figure 10 shows the mass-weighted stellar age and metallicity gradient for the final output of our simulation. It can be seen the age profile presents a minimum at roughly the position of the break. However, the metallicity profile is remarkably smooth all the way out  $\sim 15$  kpc, without any visible change at the break radius. Therefore, the U-shape of the colour profiles seen in previous section is due to an age effect, and not to a metallicity effect.

### 4.5 Evolution of the break with redshift

Several studies have now analysed the empirical evolution of the break radius with redshift (Pérez 2004; Trujillo & Pohlen 2005; Azzollini et al. 2008b). Using a sample in excess of 200 galaxies, for example, Azzollini et al. suggest that, for a given stellar mass, the radial position of the break has increased with cosmic time by a factor of  $1.3 \pm 0.1$  between  $z \sim 1$  and  $\sim 0$ . They also found that, in the same period of time, the evolution of the surface brightness level in the rest-frame B-band at the break radius ( $\mu_{br}$ ) has decreased by  $3.3 \pm 0.2$  mag arcsec $^{-2}$ .

Because the mass of our simulated galaxy evolves with redshift, we cannot compare directly the evolution of these parameters for a galaxy with a given mass. For this reason we re-analysed these data (kindly provided by the authors). We separated the observational data into three redshift bins and fitted, at each redshift, a linear relation between  $R_{br}$ ,  $\mu_{br}$ , and the mass of the galaxies, in an identical fashion to that done by Azzollini et al. (2008). Using the linear fit, we measured the predicted values of  $R_{br}$  and  $\mu_{br}$  for a galaxy

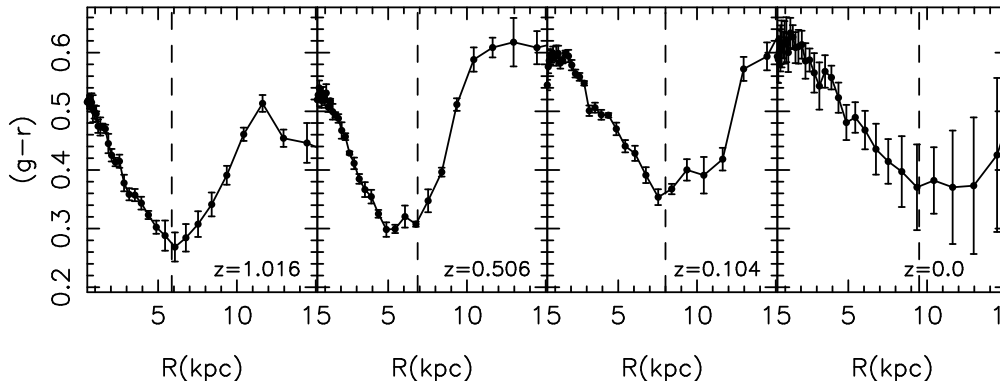


**Figure 9.** Colour profiles for several outputs of our simulation from  $z = 1$  to  $z = 0$ . Dashed lines in each panel indicate the position of  $R_{\text{br}}$  in the V-band surface brightness profile (recall, Figure 4). Error bars reflect the RMS dispersion of the mean azimuthally-averaged colour in randomly-selected octants of the disc. The colour profiles show a minimum at the break radius, in agreement with observation.

with the same mass as our disc at each of the different redshift bins (note that the mass is different at each redshift) and their associated RMS dispersions. Figure 11 shows the predicted evolution of  $R_{\text{br}}$  and  $\mu_{\text{br}}$  in the B-band for our simulated disc, compared to the observed data. It can be seen that the evolution of these parameters within our simulated disc are very similar to that which is observed.

#### 4.6 Age and metallicity distribution in the outskirts

Studies of stellar population in the outskirts of discs have found stellar populations which are of old-to-intermediate ages, with metallicity distributions peaking at relatively high metallicities ( $[\text{Fe}/\text{H}] \sim -0.7$ ) (e.g., Ferguson & Johnson 2001 (M31); Davidge 2003 (NGC 2403, M33); Galleti et al. 2004 (M33)). It has been suggested that these properties are not expected in CDM models (e.g., Ferguson & Johnson 2001), where the disc grows inside-out and at relatively recent epochs ( $z \lesssim 1$ ). Figure 12 shows the age and metallicity distributions of stars with  $R_{\text{br}} < r < 15$  kpc in our simulated disc. There is a very large scatter in the ages of the stars and a significant fraction of the stellar population has ages in excess of  $\sim 8$  Gyr. The peak of the metallicity distribution is near  $[\text{Fe}/\text{H}] \sim -0.5$  – i.e., even larger metallicities than that normally observed in the outskirts of galaxies. However, it should be noted that the “observed” metallicities are inferred via the use of colour-magnitude diagrams. When dealing with photometric metallicities, one must bear in mind that the underlying age distribution may affect the derived metallicity distribution. All of the studies cited above obtained their metallicities by comparing with the sequences of old Milky Way globular clusters. If a scatter in age is allowed, with a larger fraction of young stars (as we obtain in our simulation), the metallicity distribution will be skewed towards higher values and more closely resemble our derived distribution. We note that our metallicity distribution has a metal-poor tail, as reported in some empirical studies (e.g., Galleti et al. 2004).

## 5 BREAK FORMATION

As foreshadowed in Section 1, there is no clear consensus regarding the underlying physical mechanism responsible for the surface brightness profile breaks observed both locally and at high-redshift. Broadly, there are two categories of theories – those related with the angular momentum distribution of the stars and those related to star formation thresholds.

In our simulated disc, the break is seen in the light profile, but not in the stellar mass density profile. This indicates (or at least suggests) that the break in our disc is likely related to a change in the stellar population properties and, therefore, with a star formation threshold. The third and fourth rows of Figure 4 show the SFR density (with the SFR averaged over the last 1 Gyr) and gas surface density profiles, respectively. Examining Figure 4, we can see that the gas surface density at the break radius is not the same at all redshifts. For example, at  $z = 2.01$  there is no clear break in the surface brightness profile, despite the gas surface density reaching values significantly below the star formation threshold. This would seem to contradict the aforementioned star formation threshold scenario as the driver behind the break. In Roškar et al. (2008), the reason for the break was a sudden decrease in the gas density, but also, in agreement with our results, the density of the gas at that radius was higher than the star formation threshold imposed in their simulations. In their work, the decrease in the stellar density was due to an angular momentum limitation. By construction, in their simulations, the angular momentum is directly proportional to the radius, which means that the high angular momentum material will take longer to cool. Therefore, the angular momentum determines the maximum extent of the gaseous disc and of the star-forming disc. In fully cosmological simulations, however, the accretion of matter is not as regular as the classical model of spherical shells collapsing from increasingly large radii. Particularly, at high-redshift, before the galaxy is large enough to shock the accreting gas, accretion of gas occurs along filaments, as well as in mergers and clumps. The growth of our simulated disc is thus significantly more complicated than the disc in Roškar et al.’s idealised models. Although our disc does grow “inside-out”, it does so in a less regular manner. In our simulations, in fact, the gaseous disc extends beyond

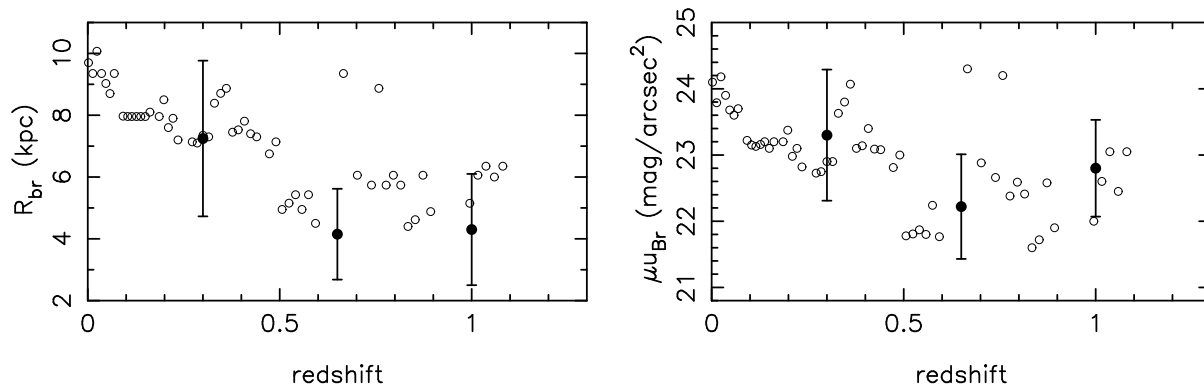


**Figure 11.** Predicted evolution with redshift of  $R_{\text{br}}$  and  $\mu_{\text{br}}$  (open circles) compared to the observed values from Azzolini et al. (2008) (filled circles with error bars). The error bars show the RMS-dispersion of the measured values for galaxies in a given redshift- and mass-bin.

the stellar disc and, while in *some* timesteps the position of the break coincides with a change of slope in the surface gas density profile, this is not true at *all* timesteps.

Ferguson et al. (1998) proposed that the breaks in the star formation density could be due to an intrinsic correlation between azimuthally-averaged star formation rate and gas volume density, combined with a vertical flaring of the disc or a warp, in such a way that the transformation between gas surface density and volume density varies with galactocentric radius (Madore et al. 1974). We plot, in Figure 14, the ratio between the surface density and the volume density of the gas in our simulated galaxy. It can be seen that, indeed, there is a change in the slope of this ratio at (approximately) the break radius.

Drops in the surface density of the gas at the onset of a warp have been observed in several galaxies (Józsa 2007; García-Ruiz et al. 2002). In fact, a possible connection between truncated profiles and gaseous warps has been suggested several times in the literature (van der Kruit 2007). Figure 13 shows the edge-on projection of the gas density distribution of our disc at three different redshifts, matching those of Figure 4. The break radius coincides with the onset of a warp in the gaseous distribution in each of these three time-steps. Therefore, the decrease in the gaseous volume density due to this flaring seems to be a fundamental mechanism responsible for the break seen in the average star formation rate and, hence, the break in the light profile.

The coincidence of the initiation of the warp with the break radius at different timesteps is an encouraging piece of evidence in support of this suggestion. Having said that, this is but one simulation; a definitive statement awaits the analysis of a systemic suite of 20-30 comparable simulations, sampling a range of environments, assembly histories, and dynamical masses – such an ambitious program is currently underway within our group.

## 6 RADIAL MIGRATION

Figure 15 compares the final (at  $z=0$ ) galactocentric radii for stars in our simulated disc ( $R_{\text{final}}$ ) with the radius at which they were formed ( $R_{\text{initial}}$ ). The right panel shows the same distribution, but only for those stars outside the break radius. Using disc stars with  $R_{\text{br}} < r < 15$  kpc, we

find that  $\sim 57\%$  of the stars formed inside the break radius,  $\sim 21\%$  formed *in situ*, and  $\sim 22\%$  formed at  $r > 15$  kpc or  $|z| > 3$  kpc, including those formed elsewhere in external satellites – i.e., more than half of the stars currently in the outskirts of the disc formed at lower radii.

The mean radial distance traversed by the disc star particles (all those with  $3 < r < 15$  kpc and  $|z| < 3$  kpc, discounting those formed in satellites for this calculation) is  $\langle |R_{\text{final}} - R_{\text{initial}}| \rangle = 1.7$  kpc, while for those with  $R_{\text{br}} < r < 15$  kpc, this mean radial traversal distance is 3.4 kpc. It is clear that in our simulation there is considerable radial migration of stars towards the external parts. The importance of such radial migration and mixing within the thin disc has been the subject of several important studies (e.g. Spitzer & Schwarzschild 1953; Barbanis & Woltjer 1967; Fuchs 2001; Sellwood & Binney 2002; Roškar et al. 2008; Haywood 2008).

It has been known for a number of years that scattering by spiral structure and molecular clouds can gradually heat stellar discs, moving stars towards more inclined and eccentric orbits and changing the overall angular momentum distribution of the disc. Minor mergers and accretion of satellites can also produce heating (e.g., Velazquez & White 1999, amongst many others). Stars that are on eccentric orbits are at different radii at different phases of their orbits and, therefore, tend to naturally produce some radial mixing. However, the radial excursions due to this mechanism are not sufficient to explain the flat age-metallicity relation in the solar neighbourhood (Sellwood & Binney 2002). Typical radial variations for a population of stars with a radial velocity dispersion  $\sigma_r$  are  $\Delta R \sim \sqrt{2}\sigma_r/k$ , where  $k$  is the epicyclic frequency; for the old stars in the Milky Way the maximum value for the excursions near the Sun is  $\sim 1-1.5$  kpc.

Another proposed mechanism for radial migration was called “churning” by Sellwood & Binney (2002), and is due to scattering of stars across co-rotation resonance by spiral waves (Sellwood & Binney 2002; Sellwood & Preto 2002; Sellwood & Kosowsky 2002; Roškar et al. 2008), resulting in a change in the orbit centres, but not the eccentricity. Such churning causes little increase in random motions (or heating) because it preserves the overall distribution of angular momentum (see Sellwood & Binney 2002 for details). In the work of Roškar et al. (2008), it was this churning mechanism that was predominantly responsible for the radial migration.



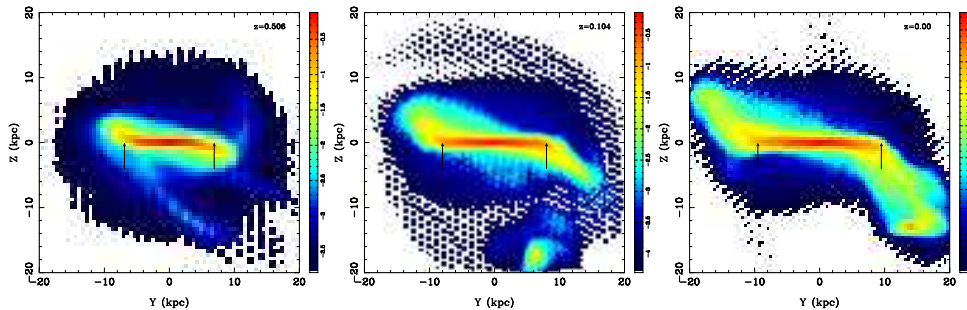


**Figure 13.** Edge-on projections of the logarithmic hydrogen density in  $\text{H cm}^{-3}$ , at three different redshifts (noted in the inset to each panel). Vertical arrows indicate the position of the break in the associated V-band stellar surface brightness profiles.

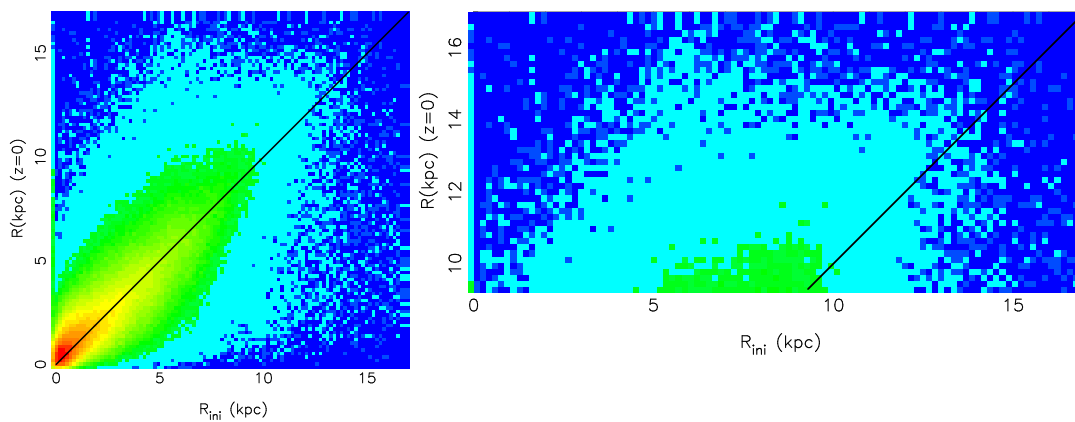


**Figure 15.** Final stellar galactocentric radius versus formation radius. The different panels correspond to different scalings on the abscissa.

Our cosmological disc (as all hydrodynamical cosmological discs to date have been) is significantly hotter than that of the Milky Way (Gibson et al. 2008); as such, radial excursion of stars in eccentric orbits is no doubt contributing to (and perhaps dominating) the mixing. In fact, the epicyclic radius of the outer disc particles is 3.3 kpc, compatible with the mean calculated  $\Delta R$ . We expect radial churning to have an important contribution too, although due to the larger scale-height of our disc, this contribution is certainly less important than in Roškar et al. (2008). Furthermore, our cosmological disc is continuously being bombarded by small satellites. Younger et al. (2007) showed that merger-driven gas inflows deepen the central potential and contract the inner profile while, at the same time, angular momentum is transferred to large radius and causes the outer disc to expand. This has the net effect of driving radial migration of the stars towards the external parts. It is very difficult to disentangle all the different causes of radial migration in our cosmological disc,<sup>5</sup> although it is certainly the case that each of these mechanisms is playing a role in both our simulated disc and in real galaxies. The main heating mechanisms in the disc presented here and in other cosmological simulations will be the subject of a future paper (House et al. 2009, in preparation).

Roškar et al. (2008) showed that radial migration due to this churning mechanism was able to explain the exponential decay of the surface brightness profile beyond  $R_{\text{br}}$ , the constancy of the break radius for stars of different ages, and predict age profiles in agreement with observations (Bakos et al. 2008). The simulation of Roškar et al. (2008) was performed under idealised conditions, with the disc growing *by construction* in an inside-out fashion, with very little star formation outside  $R_{\text{br}}$  (which itself increases monotonically with time). Hence, the stars beyond the break in their model *must* have migrated there. While these controlled, high resolution simulations are *necessary* to study many of dynamical processes having place on the disc, it is also interesting (and important) to study the evolution of the surface brightness profile within a fully cosmological context, where hot and cold modes of gas accretion, and the effects of mergers and interactions are included. We find that the break radius does not always increase monotonically with time (see, e.g., Figure 11) and the shape of the final profile is influenced by a variety of external processes. Therefore, in the next section, we explore the effect of radial migration on the overall properties of our simulated disc.

<sup>5</sup> Indeed, due to the large velocity dispersion of the stars compared with the Milky Way and to the larger scale-height, cosmological simulations may not be the most appropriate for studying these particular mechanisms.

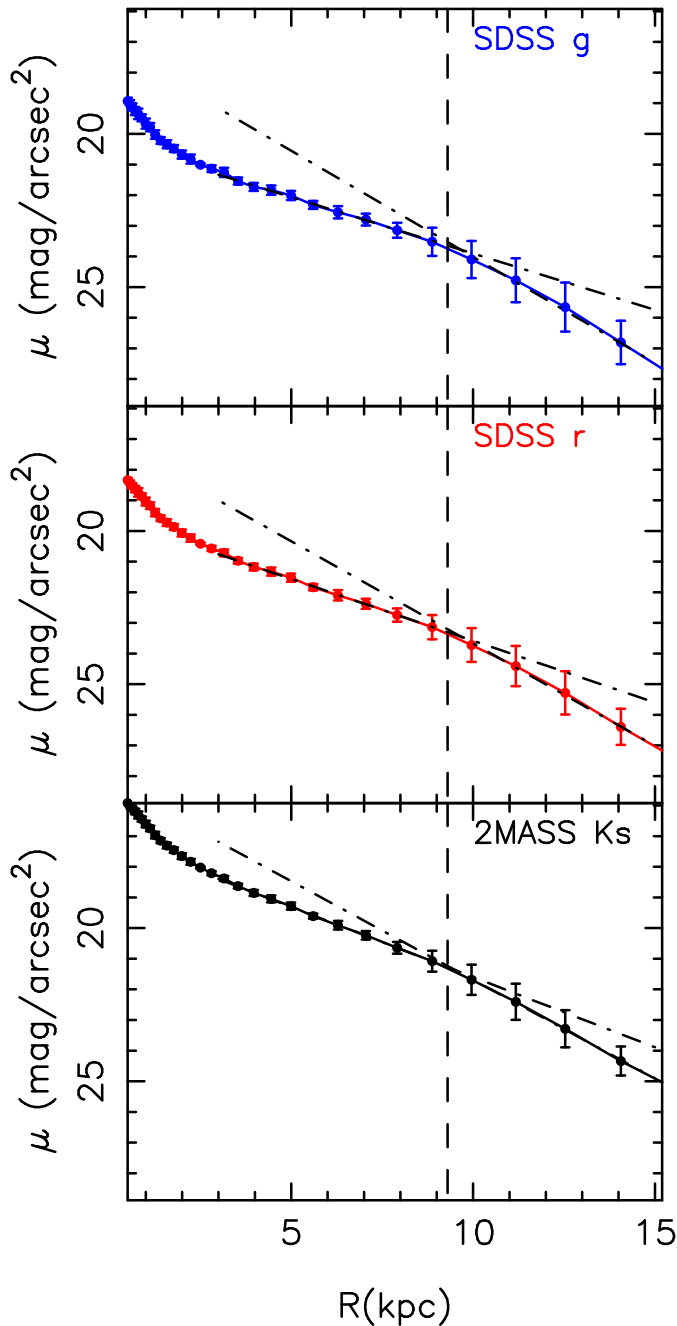


**Figure 7.** Surface brightness profiles measured in three different bands, as indicated in the inset to each panel. Dashed vertical lines show the position of the break radius, while the dashed-dotted lines represent the fits to the inner and outer exponentials.

## 7 IMPLICATIONS OF RADIAL MIGRATION FOR DISC PROPERTIES

### 7.1 Density profile

What is the effect of the radial migration in the density profile of our simulated disc? Figure 16 shows the mass density profile at  $z = 0$  compared with the hypothetical density profile that we would observe if the stars had not migrated from their birth place. The most dramatic changes in the density profile happen in the outer parts. The movement of the stars

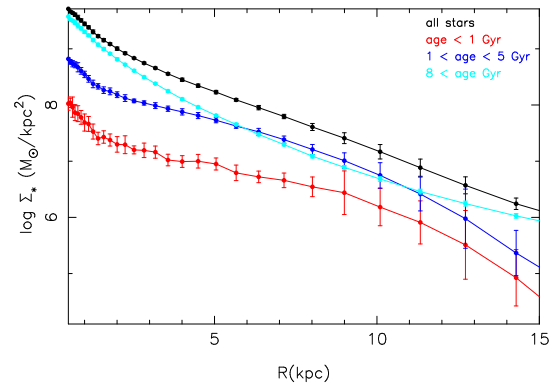


**Figure 8.** Stellar surface density profiles for stars of different ages, as noted in the inset. The intensity of the break decreases with increasing age of the stellar population under consideration, with old stars showing an “upbend” at large radii. The total stellar surface density profile is consistent with a pure exponential out to  $\sim 5$  exponential scale-lengths.

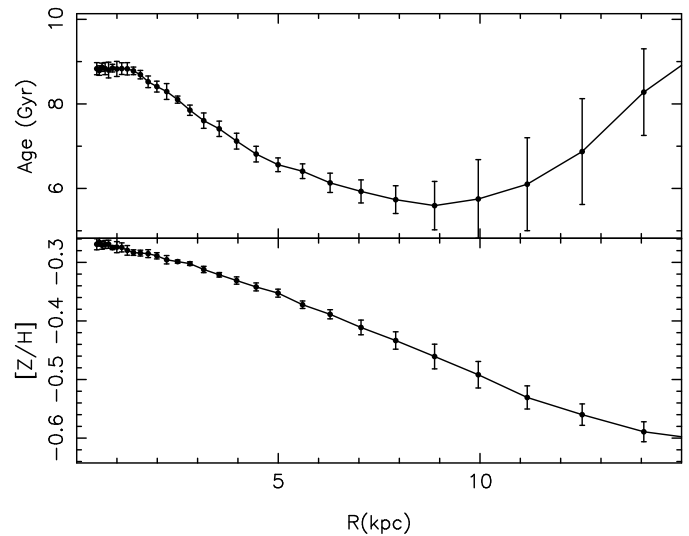


**Figure 10.** Mass-weighted age and metallicity gradients for our simulated disc at  $z=0$ .

tends to weaken the intensity of the break that would have otherwise been seen in the stellar mass density profile.

This behaviour is quite different to what is seen in the simulations where the redistribution of angular momentum is caused by a bar (eg., Foyle et al. 2008). Foyle et al. found that the outer profile in their simulations barely changed with time, while the inner profile became flatter due to the redistribution of material. Nevertheless, Pohlen & Trujillo (2006) distinguish two types of Type II profiles – those associated with the Outer Lindblad Resonance (OLR), and thus linked with the presence of a bar, and those not associated with bars, which are normally located at large radius (see Erwin et al. 2008 for a more detailed discussion). It may well be that two different mechanism are responsible for these two variants of the Type II profiles. The profiles not associated with the OLR are less common in early-type galaxies than late-type galaxies (Pohlen & Trujillo 2006) which may indicate that the presence of an extended gaseous disc are necessary to produce them.

We showed, in Sec. 4.2, that the old stars have a density

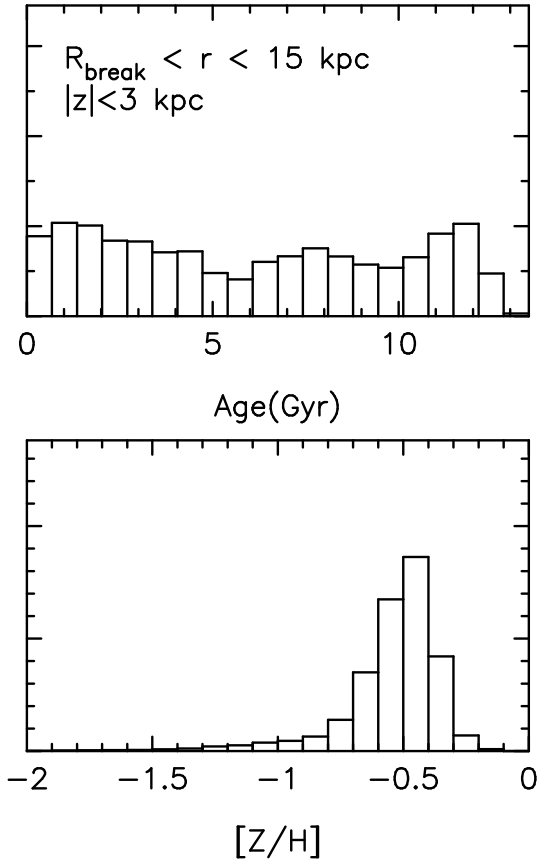


**Figure 12.** Age and metallicity distributions for the stars with radius  $R_{\text{br}} < r < 15$  kpc and  $|z| < 3$  kpc.

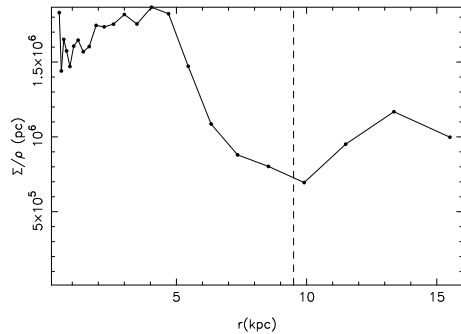


**Figure 14.** Ratio between the surface mass density and the volume density, as a function of galactocentric radius at redshift  $z=0$ , in our simulated disc galaxy. The position of the break in the surface brightness profile is indicated with a dashed line.

profile with an upturn in the outer parts. Figure 17 demonstrates that this is partially due to the significant effect that migration has on this outer profile. In this figure, the stellar density profile using different age bins is compared with the same profiles in the hypothetical situation where the stars have not migrated from the place of their birth. It is readily apparent that the surface density profile, in the absence of migration, appears truncated in all cases. This contrasts with the mass density profiles that we derived from the final output of our simulation, which appear much closer to a pure exponential (to at least  $\sim 5$  exponential scale lengths). We conclude, therefore, that the exponential mass den-

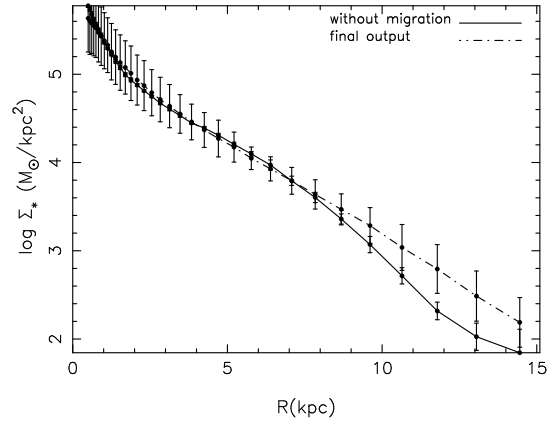


**Figure 16.** Stellar surface brightness density profile of the disc at  $z=0$  (dot-dashed curve) compared with the profile the disc would possess in the hypothetical situation that the redistribution of stellar material by secular processes was absent.

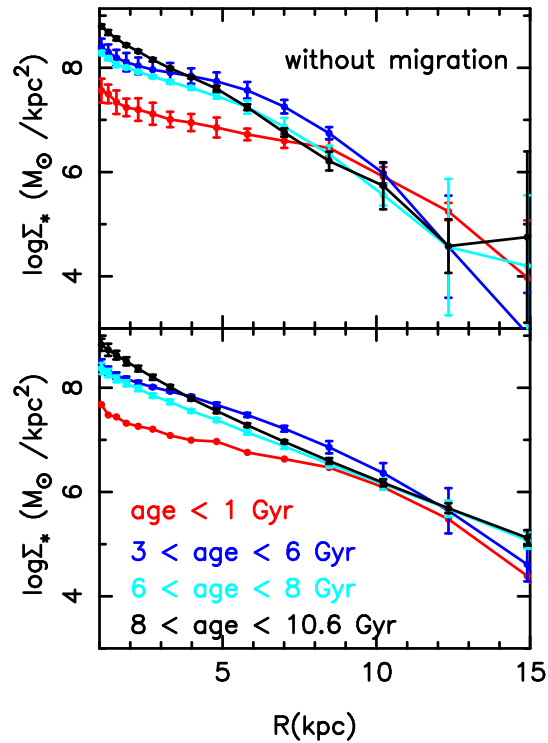


**Figure 17.** As in Figure 16, but subdividing the stars by age, as indicated in the inset to each panel; upper panel: hypothetical situation of no radial migration; lower panel: as measured in our cosmological simulation.

sity profile in Figure 4 would appear truncated/broken if there had not been radial migration. As old stars have had more time to migrate towards the external parts, the density profile for the oldest age bin appears anti-truncated. This mechanism could also be responsible for the upbending profiles seen in galaxies where a truncation in the star formation density does not occur (Type III profiles, recalling the nomenclature of Section 1). This was also proposed by Younger et al. (2007) who found that in their simulations, the radial migration was produced by angular momentum transfer during minor mergers; such a scenario receives

support from the empirical evidence associating asymmetries and distortions with anti-truncated discs (Erwin 2005; Pohlen & Trujillo 2006). As mentioned in Section 6, several mechanisms are certainly operating in our disc, in order to produce the radial migration of stars toward the external parts, including this effect of satellite accretion.

## 7.2 Stellar populations

Stars and interstellar gas in galaxies exhibit diverse chemical element abundance patterns that are shaped by their environment and formation histories. A wealth of surveys and satellite missions are devoted to obtain chemical patterns for individual stars as well as ages and kinematics in order to derive the star formation history and merger history of our galaxy (e.g., HIPPARCOS, RAVE, SEGUE, GAIA). The comparison with chemical and chemodynamical evolution models is expected to provide insights into the formation epoch of the different Galactic components and the relation between them.

Chemical evolution models of the Milky Way usually divide the "Galaxy" into annuli with no radial transfer of material between them (e.g. Fenner & Gibson 2003; Chiappini et al. 2003). However, recent works (e.g. Roškar et al. 2008b; Schönrich & Binney 2008; Haywood 2008) has pointed out the importance that migration mechanisms might have in the studies of chemical evolution, in particular, upon the observational constraints used to calibrated the models. For example, one of the most difficult observational results to reproduce with current "semi-numerical" chemical evolution models is the lack of an apparent correlation between the age and the metallicity of the stars in the solar neighbourhood, as well as the large scatter in metallicity at a given age. On the other hand, full chemodynamical models indicate that radial migration might be an explanation to this lack of correlation. Roškar et al. (2008) have shown that radial migration can largely affect the age and metallicity gradients, as well as the dearth of metal-poor stars in the solar neighbourhood (the so-called "G-dwarf problem"). It has even been suggested that radial migration might be responsible for the formation of the thick disc (e.g. Schönrich & Binney 2008, Haywood 2008).

These studies provide the motivation to re-examine the stellar population distribution within our simulated disc, where infall of material and the accretion of satellites are taken into account naturally within our cosmological framework.

### 7.2.1 The age-metallicity relation

Chemical evolution models predict an increase of the metal content in the ISM as stellar generations die and pollute their surroundings with the byproducts of nucleosynthesis. One might expect therefore that the youngest (oldest) stars would also be the most metal-rich (metal-poor). However, there is little evidence of such an age-metallicity relation in the solar neighbourhood (Feltzing et al. 2001; Nordström et al. 2004). Furthermore, the scatter in the relation is very large – i.e., at a given age, there is a large spread in the metallicity distribution. Classically, this was interpreted as a result of inefficient mixing of stellar

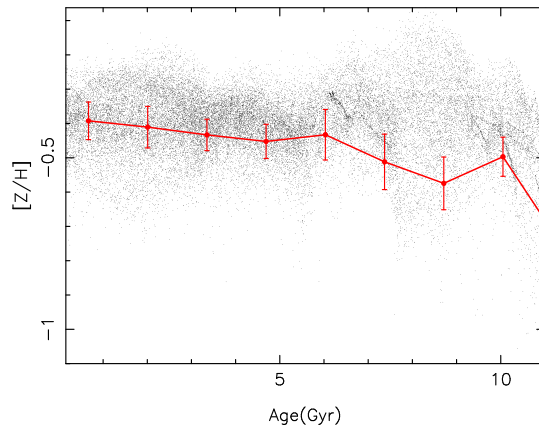


**Figure 18.** Age-metallicity relation for stellar particles with radius between 7 and 9 kpc and scale-height  $|z| < 3$  kpc, chosen to represent a region roughly corresponding to the "solar neighbourhood". The red points indicate the values derived for the stars born in this region.

ejecta. However, several authors (e.g., Wielen et al. 1996; Sellwood & Binney 2002) have suggested the possibility that radial migration may have enabled old stars, formed at small galactocentric radii, to appear in the solar neighbourhood, flattening any correlation between age and metallicity. Roškar et al. (2008) and Schönrich & Binney (2008) have shown that a flatter age-metallicity relation and a large spread in metallicities at a given age can be obtained with dynamical models where radial mixing is taken into account. Haywood (2006, 2008) observed that stars in the metal-poor and metal-rich end of the thin disc have orbital parameters which are offset from the main population, which he interpreted as being the consequence of radial migration.

Fig. 18 shows the age-metallicity relation in the "solar neighborhood" ( $7 < r < 9$  kpc and  $|z| < 3$  kpc) of our simulated disc, compared with the age-metallicity relation that we would have measured in the absence of migration. As can be seen, our fully-cosmological study is in agreement with the aforementioned idealised models. Radial migration produces a considerable flattening, and an increase of the scatter, in the age-metallicity relation. In the absence of radial migration, the stars in the solar neighborhood of our disc would show a relation between these two parameters.

### 7.2.2 Age gradient

We showed, in Sec. 4.4 that the radial age profile has a minimum at the break radius, similar to that found by Roškar et al. (2008). In their work, the radial extent of the star forming disc was limited by the maximum angular momentum of material that was able to cool at each timestep. Therefore, by construction, the disc grows inside-out and the youngest stars are situated at the break radius. The "up-bend" in the age profile at  $r > R_{br}$  was produced, exclusively, by stars that had migrated from the internal parts of the disc. Because older stars have more time to travel larger distances, the trend of the age with radius reversed after the break radius.

To explore if this is also true in our simulation, we plot, in Fig. 19, the mass-weighted age profile that the stellar disc would have if the stars did not migrate from their birth

place, compared with that derived from the final at  $z = 0$ . As can be seen, even in the absence of radial migration, a 'U-shape' profile in the age gradient is still visible. Stellar migration changes the shape of this profile, but the increasing mass-weighted age with increasing radius in the outer parts is *not* due to radial migration. Figure 20 shows the evolution with time of the total star formation rate density for stars formed at different galactocentric radii, including regions inside and beyond the break radius. For radii  $3 < r < 5$  kpc, the SFR density decreases with time, while the opposite happens for  $5 < r < 7$  kpc. The consequence of this is that the the fraction of young-to-old stars increases with radius until  $r = R_{\text{br}}$ , consistent with expectations, as the early accreted mass has low specific angular momentum. These trends are responsible for the decreasing mean age with radius and are in agreement with the inside-out scenario for the formation of disc galaxies (Ryder & Dopita 1994). However, the trend disappears beyond the break radius, where the star formation rate is low and essentially constant throughout the evolution of the galaxy. The difference in the star formation rate between the outer ( $10 < r < 15$  kpc) and inner ( $7 < r < 9$  kpc) parts is higher at later times, and that is the main reason for the upturn in the age gradient. Another way to appreciate this is by studying the radial profile of the birth parameter, defined as the current versus averaged star formation rate  $b = (\text{SFR} / \langle \text{SFR} \rangle)$  (Kennicutt et al. 1994). Instead of plotting the current star formation rate, we averaged the star formation over the last 1 Gyr. This is mainly due to the relative few number of particles with ages below this value outside the break radius. We plot, in Fig. 21, this parameter as a function of galactocentric radius. As can be seen,  $b$  increases almost linearly with radius, as expected for an inside-out formation scenario, until the break radius, where it reaches a plateau and then decreases. The increase in the error bars at the break radius reflects the asymmetries in the age distribution of the stars beyond this radius (recall Fig. 5).

We argue that the U-shape age profile is the direct consequence of the existence of a break in the star formation density. If the star formation outside the break had not decreased suddenly, the age gradient would decrease, or remain constant, until the edge of the optical disc. This is supported by the result of Bakos et al. (2008) who only found the tell-tale U-shaped colour profiles for galaxies possessing a Type II profile. The galaxies with an essentially pure exponential profile within their sample showed a plateau (and not an up-bend) in the colours at large radii. This up-bending age profile does not mean that the disc did not form inside-out. In fact, the "overall" formation of the disc remains inside-out. However, in our disc, the decrease of star formation in the external parts – due to a decrease in the volume density of the gas – results in redder colors beyond the break radius.

In Fig. 19 we also compare the age profile of the galaxy with the one it would have if *all* the stars formed in the disc – i.e., if satellites were not accreted. It is apparent that for this case, the accretion of satellites has little effect on the stellar population gradients.

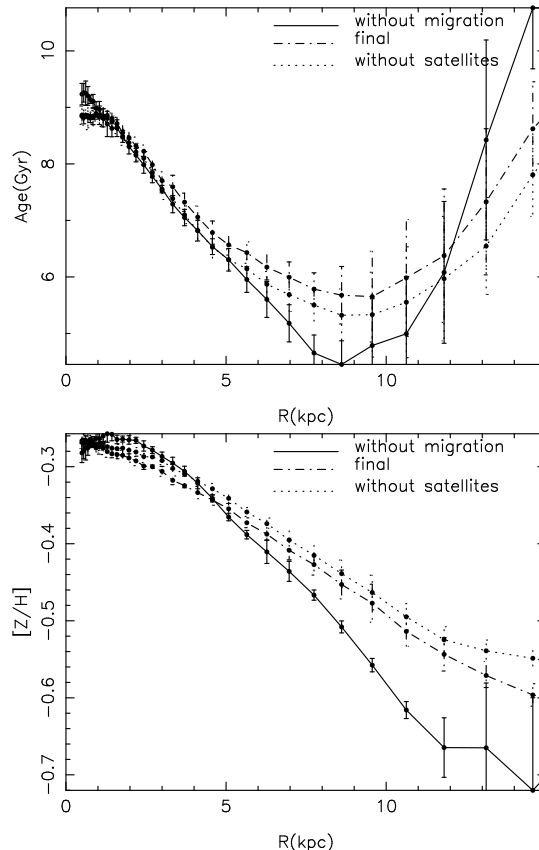


**Figure 19.** Mass-weighted azimuthally-averaged stellar age and metallicity gradients. Solid lines: Theoretical gradient for the hypothetical case were stars do not migrate from their birth place. Dashed-dotted line: Profile measured in the final timestep of our simulation. Dotted line: Profile measured in the final timestep of the simulation after eliminating those stars which formed outside the disc (those with initial galactocentric radii in excess of 25 kpc).

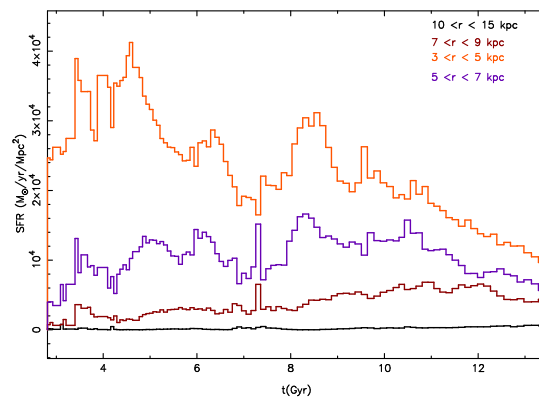


**Figure 20.** Comparison of the star formation rate density with time in 4 different regions of the galaxy disc – black: between 10 and 15 kpc; dark red: between 7 and 9 kpc; purple: between 5 and 7 kpc and orange between 3 and 5 kpc.

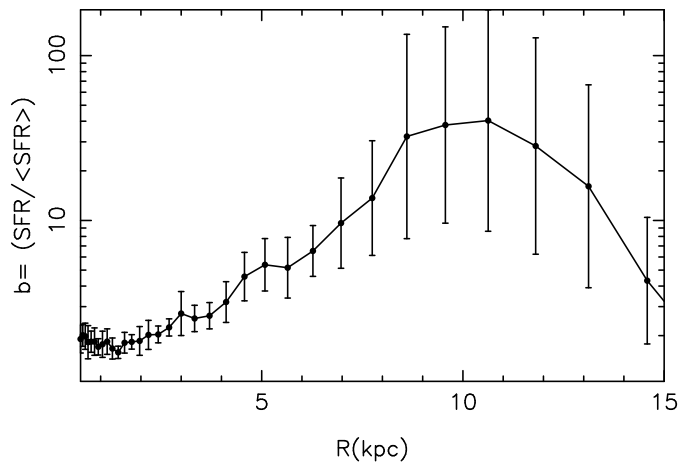


**Figure 21.** Star formation over the last 1 Gyr divided by the total mass of stars formed before this epoch (the so-called “birth rate”) as a function of galactocentric radius.

### 7.2.3 Metallicity gradient

The metallicity gradient in the disc and its evolution with time provides constraints to our understanding of the formation and evolution of galaxies. The presence of a metallicity gradient in the Milky Way is widely accepted, although its exact slope and shape remain contentious (Chiappini et al. 2001; Andrievsky et al. 2002). A related issue is the evolution of this gradient with time; this has been approached from both the theoretical (Götz & Köppen 1992; Köppen 1994; Molla et al. 1997; Henry & Worthey 1999; Chiappini et al. 2001) and observational perspectives (Friel et al. 2002; Maciel 2001; Maciel, Costa & Uchida 2003; Stanghellini et al. 2006) but it is still not clear whether the metallicity gradient in our Galaxy flattens or steepens with time. Measurements using HII regions, B-stars, and planetary nebulae, find gradients ranging from  $\sim -0.04$  to  $\sim -0.07$  dex  $\text{kpc}^{-1}$  (Deharveng et al. 2000; Afflerbach et al. 1997; Daflon & Cunha 2004; Gummersbach et al. 1998; Costa et al. 2004; Maciel & Quireza 1999, although see Stanghellini et al. 2006). Even more recently, Carraro et al. (2007), using five old open clusters, suggest an even shallower gradient of  $-0.018$  dex  $\text{kpc}^{-1}$ . There is also controversy in the literature about the shape of the gradient, including the presence or not of a discontinuity at around 10 – 12 kpc. Part of the uncertainty in this field can no doubt be traced to the necessary use of disparate tracers of the gradients, each which probe a different age (or range of ages).

In our simulations, we find that the metallicity gradient is flatter for old stars than it is for young stars, as shown in Figure 22. It can also be seen that radial migration is partially responsible for this flattening (see Fig. 19), in agreement with Roškar et al. (2008). We also predict that the optimal galactocentric radius in which to seek differences between the gradients in the old versus young populations is  $3 < r < 5$  kpc. As can be seen in Figure 19 (lower panel), the mean metallicity gradient in our simulation shows a flattening at  $r > 12$  kpc.

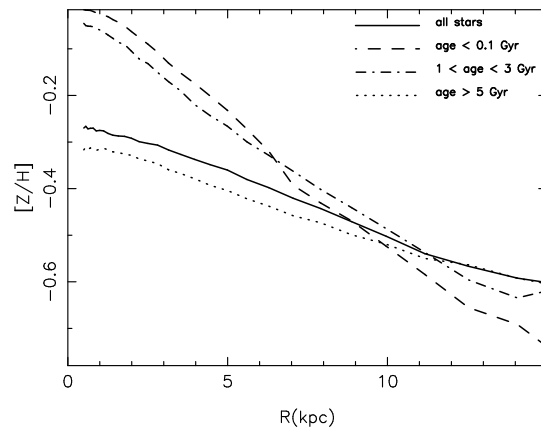


**Figure 22.** Azimuthally-averaged metallicity profile at redshift  $z=0$  for stars in different age bins, as noted in the inset.

## 8 DISCUSSION AND CONCLUSIONS

We have studied the origin of the disc truncations and the stellar population properties of a disc galaxy formed within a cosmological framework. To do this, we have analysed a multi-resolved cosmological simulation of a Milky Way-mass halo, including dark matter and gas dynamics, metallicity-dependent cooling, UV heating, star formation, and supernovae feedback, using the AMR code RAMSES. Our simulated disc shows a break in the surface brightness profile at  $\sim 3$  exponential scale-lengths, similar to those observed in a large fraction of disc galaxies. The position of the break does not coincide with the radius at which the gas density reaches the canonical threshold for star formation. In our simulation, this break in the stellar light is due to a decrease in the star formation density per unit area (averaged over the past  $\sim 1$  Gyr). This decrease in the star formation density originates from a decrease in the volume density of gas at the break radius, which itself coincides with the radius at which the gas disc begins to warp ( $R_{\text{warp}}$ ). A relationship between truncations and warps has been pointed out by several studies (see van der Kruit 2008 for a review as well as van der Kruit 2001). van der Kruit (2007) found that the distribution of  $R_{\text{warp}}/R_{\text{br}}$  in a sample of SDSS galaxies was statistically consistent with all warps starting at  $\sim 1.1 R_{\text{br}}$ . Our simulation is entirely consistent with these observations. At a first sight, therefore, it seems that the presence of a warp is a condition for the presence of a break in the stellar light distribution. However, we re-iterate that this need to be confirmed with a larger sample of simulated and observed discs.

We analysed the redistribution of material and angular momentum in the disc, finding that it affects considerably the final shape of the mass density profile, especially in the outskirts. In fact, 57% of the stars with  $r > R_{\text{br}}$  formed at lower radii. The reason why the surface density profile does not show a truncation similar to the one observed in the stellar light is traced to this migration of stars towards the outer disc. We suggest that truncated and anti-truncated profiles can be produced by a different combination of two processes: (1) a change in the slope of star formation profile with radius due to a change of the slope in the gas density profile (which causes the truncation in the light), and (2) radial migration of stars formed in the internal parts towards radii in excess of  $R_{\text{br}}$ . We speculate that up-bending profiles can be

produced in our simulation when the distribution of the gas changes smoothly with radius. In that case, process (1) is suppressed, the star formation rate per unit area in the disc changes smoothly with radius, and the only deviations from a pure exponential profile are due to stars migrating from disc interior, producing an increase in both the surface light and mass density in the external parts. This would make the external parts somewhat redder, in agreement with observations (Bakos et al. 2008). Pure exponential profiles can be similar to anti-truncated profiles, but with less migration.

We have also studied the stellar populations in the disc and the influence of the migration of stars and the accretion of satellites in the age and metallicity profiles. We found, in agreement with recent observations (Bakos et al. 2008) that the disc shows a U-shaped age profile, reaching the minimum age at the position of the break. It has been proposed in recent works that this profile is produced by the combination of two processes: (1) the inside-out growth of the disc (resulting in the age decreasing with radius until  $R_{br}$ ), and (2) the migration of old stars from the interior to the exterior parts of the disc beyond  $R_{br}$ . In this picture, the increase of age with radius beyond the break results from older stars having more time to travel from the inner disc and, therefore, reach a greater galactocentric radius. These models predict a flat metallicity gradient for the old stellar populations, as these stars are mixed very efficiently. In our simulation, the U-shaped profile is due to a different rate of star formation between the internal and the external regions (inside and outside the break radius). Migration of the stars also has an impact on this profile, but the U-shape age profile with the minimum at the break radius appears even when migration is suppressed in the disc. We find that the U-shaped age profile is due to the same mechanism as the one producing the break in the surface brightness distribution - ie, a diminution of the star formation rate in the external region, due to the warping of the gaseous disc and, therefore we predict that this type of color profile is only present when there is a break in the light distribution. This is in agreement with the recent work of Bakos et al. (2008), at low redshifts, and Azzollini et al. (2008) at redshifts out to  $z \sim 1.1$ .

The distribution of ages in the outer disc of our simulation is very broad with stars nearly as old as the age of the Universe itself. The presence of old stars ( $>10$  Gyr) in the outer disc of some nearby galaxies, such as M31 (Ferguson & Johnson 2001), has been used as an argument against  $\Lambda$ CDM models, arguing that, if feedback is included in order to produce large discs, the formation of the disc is delayed and the resulting stellar populations should be of young and intermediate ages. We show here that in a  $\Lambda$ CDM framework we were able to produce disc with both a realistic scale-length and a considerable number of old stars in its external parts. The metallicity distribution of stars in the outskirts of the disc peaks at  $[Fe/H] \sim -0.5$  and shows also a significant spread, also consistent with observations.

Finally, we studied the age-metallicity relationship in a representative "solar neighbourhood" of our simulation. There have been claims suggesting that radial mixing of stars might be responsible for the absence of an obvious correlation between these two parameters in the solar neighbourhood, and for the large scatter in metallicity at a given age. We agree with these claims, showing that a flat relationship between age and metallicity, and significant scatter

in metallicity at a given age, are a natural outcome within our cosmological simulation.

In a forthcoming paper we will study the origin of the warp in the gaseous distribution, its lifetime, asymmetry, and intensity. This will be supplemented with a suite of 20-30 additional disc simulations, spanning a range of mass, environment, and assembly history. This will allow us to provide significantly more robust predictions for the relationship between break radii and other empirical characteristics of galaxies.

## ACKNOWLEDGMENTS

We wish to thank Romain Teyssier, Ignacio Trujillo, Armando Gil de Paz, and Isabel Pérez, for their constant and extremely enlightening advice. We thank Ruyman Azzolini for providing his data in tabular form and the referee of this paper, Dr Peter Erwin for useful comments that have improved the presentation of the manuscript. We also thank Victor Debattista and Rok Roškar for useful comments that improved significantly the manuscript. PSB acknowledges the support of a Marie Curie Intra-European Fellowship within the 6th European Community Framework Programme. BKG acknowledges the support of the UK's Science & Technology Facilities Council (STFC Grant ST/F002432/1) and the Commonwealth Cosmology Initiative. All modeling and analysis was carried out on the University of Central Lancashire's High Performance Computing Facility and the UK's National Cosmology Supercomputer (COSMOS).

## REFERENCES

- Abadi M. G., Navarro J. F., Steinmetz M., Eke V. R., 2003a, *ApJ*, 591, 499
- Abadi M. G., Navarro J. F., Steinmetz M., Eke V. R., 2003b, *ApJ*, 597, 21
- Afflerbach A., Churchwell E., Werner M. W., 1997, *ApJ*, 478, 190
- Andrievsky S. M., Kovtyukh V. V., Luck R. E., Lépine J. R. D., Maciel W. J., Beletsky Y. V., 2002, *A&A*, 392, 491
- Azzollini R., Trujillo I., Beckman J. E., 2008a, *ApJ*, 679, L69
- Azzollini R., Trujillo I., Beckman J. E., 2008b, *ApJ*, 684, 1026
- Bakos J., Trujillo I., Pohlen M., 2008, *ApJ*, 683, L103
- Barbanis B., Woltjer L., 1967, *ApJ*, 150, 461
- Barton I. J., Thompson L. A., 1997, *AJ*, 114, 655
- Bell E. F., McIntosh D. H., Katz N., Weinberg M. D., 2003, *ApJS*, 149, 289
- Bland-Hawthorn J., Vlajić M., Freeman K. C., Draine B. T., 2005, *ApJ*, 629, 239
- Carraro G., Geisler D., Villanova S., Frinchaboy P. M., Majewski S. R., 2007, *A&A*, 476, 217
- Chiappini C., Matteucci F., Romano D., 2001, *ApJ*, 554, 1044
- Chiappini C., Romano D., Matteucci F., 2003, *MNRAS*, 339, 63

- Costa R. D. D., Uchida M. M. M., Maciel W. J., 2004, *A&A*, 423, 199
- Daflon S., Cunha K., 2004, *ApJ*, 617, 1115
- Dalcanton J. J., Spergel D. N., Summers F. J., 1997, *ApJ*, 482, 659
- Davidge T. J., 2003, *AJ*, 125, 3046
- de Grijs R., Kregel M., Wesson K. H., 2001, *MNRAS*, 324, 1074
- de Jong R. S., Seth A. C., Radburn-Smith D. J., Bell E. F., Brown T. M., Bullock J. S., Courteau S., Dalcanton J. J., Ferguson H. C., Goudfrooij P., Holfeltz S., Holwerda B. W., Purcell C., Sick J., Zucker D. B., 2007, *ApJ*, 667, L49
- Debattista V. P., Mayer L., Carollo C. M., Moore B., Wadsley J., Quinn T., 2006, *ApJ*, 645, 209
- Deharveng L., Peña M., Caplan J., Costero R., 2000, *MNRAS*, 311, 329
- Dubois Y., Teyssier R., 2008, *A&A*, 477, 79
- Elmegreen B. G., Hunter D. A., 2006, *ApJ*, 636, 712
- Erwin P., Beckman J. E., Pohlen M., 2005, *ApJ*, 626, L81
- Erwin P., Pohlen M., Beckman J. E., 2008, *AJ*, 135, 20
- Fall S. M., Efstathiou G., 1980, *MNRAS*, 193, 189
- Feltzing S., Holmberg J., Hurley J. R., 2001, *A&A*, 377, 911
- Fenner Y., Gibson B. K., 2003, *PASA*, 20, 189
- Ferguson A. M. N., 1998, PhD thesis, Johns Hopkins University
- Ferguson A. M. N., Clarke C. J., 2001, *MNRAS*, 325, 781
- Ferguson A. M. N., Johnson R. A., 2001, *ApJ*, 559, L13
- Ferguson A. M. N., Wyse R. F. G., Gallagher J. S., Hunter D. A., 1998, *ApJ*, 506, L19
- Ferland G. J., Korista K. T., Verner D. A., Ferguson J. W., Kingdon J. B., Verner E. M., 1998, *PASP*, 110, 761
- Foyle K., Courteau S., Thacker R. J., 2008, *MNRAS*, 386, 1821
- Freeman K. C., 1970, *ApJ*, 160, 811
- Friel E. D., Janes K. A., Tavares M., Scott J., Katsanis R., Lotz J., Hong L., Miller N., 2002, *AJ*, 124, 2693
- Fuchs B., 2001, *MNRAS*, 325, 1637
- Galletti S., Bellazzini M., Ferraro F. R., 2004, *A&A*, 423, 925
- García-Ruiz I., Sancisi R., Kuijken K., 2002, *A&A*, 394, 769
- Gil de Paz A., Madore B. F., Boissier S., Thilker D., Bianchi L., Sánchez Contreras e. a., 2007, *ApJ*, 661, 115
- Goetz M., Koeppen J., 1992, *A&A*, 262, 455
- Governato F., Willman B., Mayer L., Brooks A., Stinson G., Valenzuela O., Wadsley J., Quinn T., 2007, *MNRAS*, 374, 1479
- Gummersbach C. A., Kaufer A., Schaefer D. R., Szeifert T., Wolf B., 1998, *A&A*, 338, 881
- Haywood M., 2006, *MNRAS*, 371, 1760
- Haywood M., 2008, *MNRAS*, 388, 1175
- Henry R. B. C., Worthey G., 1999, *PASP*, 111, 919
- Hunter D. A., Elmegreen B. G., 2006, *ApJS*, 162, 49
- Jansen R. A., Fabricant D., Franx M., Caldwell N., 2000, *ApJS*, 126, 331
- Józsa G. I. G., 2007, *A&A*, 468, 903
- Kennicutt Jr. R. C., Tamblyn P., Congdon C. E., 1994, *ApJ*, 435, 22
- Koeppen J., 1994, *A&A*, 281, 26
- Kregel M., van der Kruit P. C., de Grijs R., 2002, *MNRAS*, 334, 646
- Maciel W. J., 2001, *New Astronomy Review*, 45, 571
- Maciel W. J., Costa R. D. D., Uchida M. M. M., 2003, *A&A*, 397, 667
- Maciel W. J., Quireza C., 1999, *A&A*, 345, 629
- Madore B. F., van den Bergh S., Rogstad D. H., 1974, *ApJ*, 191, 317
- Maraston C., Thomas D., 2000, *ApJ*, 541, 126
- Mo H. J., Mao S., White S. D. M., 1998, *MNRAS*, 295, 319
- Molla M., Ferrini F., Diaz A. I., 1997, *ApJ*, 475, 519
- Navarro J. F., White S. D. M., 1994, *MNRAS*, 267, 401
- Nordström B., Mayor M., Andersen J., Holmberg J., Pont F., Jørgensen B. R., Olsen E. H., Udry S., Mowlavi N., 2004, *A&A*, 418, 989
- Okamoto T., Eke V. R., Frenk C. S., Jenkins A., 2005, *MNRAS*, 363, 1299
- Patterson F. S., 1940, *Harvard College Observatory Bulletin*, 914, 9
- Peñarrubia J., McConnachie A., Babul A., 2006, *ApJ*, 650, L33
- Pérez I., 2004, *A&A*, 427, L17
- Pohlen M., 2002, PhD thesis, Ruhr-Universität Bochum
- Pohlen M., Beckman J. E., Hüttemeister S., Knapen J. H., Erwin P., Dettmar R.-J., 2004, in Block D. L., Puerari I., Freeman K. C., Groess R., Block E. K., eds, *Penetrating Bars Through Masks of Cosmic Dust* Vol. 319 of *Astrophysics and Space Science Library*, *Stellar Disk Truncations: Where do we stand?*. pp 713–+
- Pohlen M., Trujillo I., 2006, *A&A*, 454, 759
- Rose J. A., 1985, *AJ*, 90, 1927
- Roškar R., Debattista V. P., Quinn T. R., Stinson G. S., Wadsley J., 2008, *ApJ*, 684, L79
- Roškar R., Debattista V. P., Stinson G. S., Quinn T. R., Kaufmann T., Wadsley J., 2008, *ApJ*, 675, L65
- Scannapieco C., Tissera P. B., White S. D. M., Springel V., 2008, *MNRAS*, 389, 1137
- Scannapieco C., White S. D. M., Springel V., Tissera P. B., 2008, *ArXiv e-prints*
- Schoenrich R., Binney J., 2008, *ArXiv e-prints*
- Sellwood J. A., Binney J. J., 2002, *MNRAS*, 336, 785
- Sellwood J. A., Kosowsky A., 2002, in Da Costa G. S., Jerjen H., eds, *The Dynamics, Structure & History of Galaxies: A Workshop in Honour of Professor Ken Freeman* Vol. 273 of *Astronomical Society of the Pacific Conference Series*, *Distinguishing Dark Matter from Modified Gravity*. pp 243–+
- Sellwood J. A., Preto M., 2002, in Athanassoula E., Bosma A., Mujica R., eds, *Disks of Galaxies: Kinematics, Dynamics and Perturbations* Vol. 275 of *Astronomical Society of the Pacific Conference Series*, *Scattering of Stars by Transient Spiral Waves*. pp 281–292
- Simien F., de Vaucouleurs G., 1986, *ApJ*, 302, 564
- Spitzer L. J., Schwarzschild M., 1953, *ApJ*, 118, 106
- Springel V., Hernquist L., 2003, *MNRAS*, 339, 289
- Stanghellini L., Guerrero M. A., Cunha K., Machado A., Villaver E., 2006, *ApJ*, 651, 898
- Teyssier R., 2002, *A&A*, 385, 337
- Thilker D. A., Bianchi L., Boissier S. e. a., 2005, *ApJ*, 619, L79
- Thilker D. A., Bianchi L., Meurer G. e. a., 2007, *ApJS*, 173, 538



- Trager S. C., Worthey G., Faber S. M., Dressler A., 2005, MNRAS, 362, 2
- Trujillo I., Pohlen M., 2005, ApJ, 630, L17
- van den Bosch F. C., 2001, MNRAS, 327, 1334
- van der Kruit P. C., 1987, A&A, 173, 59
- van der Kruit P. C., 2001, in Funes J. G., Corsini E. M., eds, Galaxy Disks and Disk Galaxies Vol. 230 of Astronomical Society of the Pacific Conference Series, Truncations in Stellar Disks. pp 119–126
- van der Kruit P. C., 2007, A&A, 466, 883
- van der Kruit P. C., 2008, in Funes J. G., Corsini E. M., eds, Astronomical Society of the Pacific Conference Series Vol. 396 of Astronomical Society of the Pacific Conference Series, The Stars and Gas in Outer Parts of Galaxy Disks: Extended or Truncated, Flat or Warped?. pp 173–+
- Weiner B. J., Williams T. B., van Gorkom J. H., Sellwood J. A., 2001, ApJ, 546, 916
- Wielen R., Fuchs B., Dettbarn C., 1996, A&A, 314, 438
- Worthey G., 1994, ApJS, 95, 107
- Younger J. D., Cox T. J., Seth A. C., Hernquist L., 2007, ApJ, 670, 269

## APPENDIX A: DEPENDENCE OF THE BREAK RADIUS UPON INCLINATION

Recently, van der Kruit (2008) studied the correlations between break radius and other galaxy properties, finding fundamental differences between the trends described by face-on and edge-on galaxies. In particular, he did not find a correlation between the position of the break and the rotational velocity in the face-on sample, while the correlation was evident in the edge-on galaxies. In principle, breaks are more easily detected in edge-on galaxies, due to their favored integrate line-of-sight vantage point. Face-on breaks are more difficult to detect and if the truncation radius changes with azimuth, the azimuthally-averaged profiles would “smear out” the intensity of the break. Furthermore, intrinsic deviations from circular symmetry, such as spiral arms (especially for younger populations) should complicate matters for less-inclined systems. On the other hand, edge-on studies are more susceptible to line-of-sight effects caused by integrating through the disc. The differences between the parameters measured in face-on and edge-on samples can be obtained statistically, but obviously, they are difficult to quantify. In this appendix, we compare the break radius and the intensity of the break in different bands by viewing our simulation various face-on and edge-on configurations, in order to quantify possible differences due to geometry. Differences due to the varying dust contribution with inclination cannot be treated here, but we refer the reader to Pohlen et al. (2008) for a thorough analysis of this issue.

All the profiles previously showed in this work have been obtained by azimuthally-averaging the luminosities of the stars within 3 kpc of the disc mid-plane. Observers, of course, integrate their luminosities along the entire line-of-sight. In order to mimic this we compare the profiles integrating the light of all stars within a distance of 10 kpc from the disc mid-plane. Figure A1 shows the surface brightness profiles in different bands obtained for face-on and edge-on orientations. Table A1 shows the measured values for the

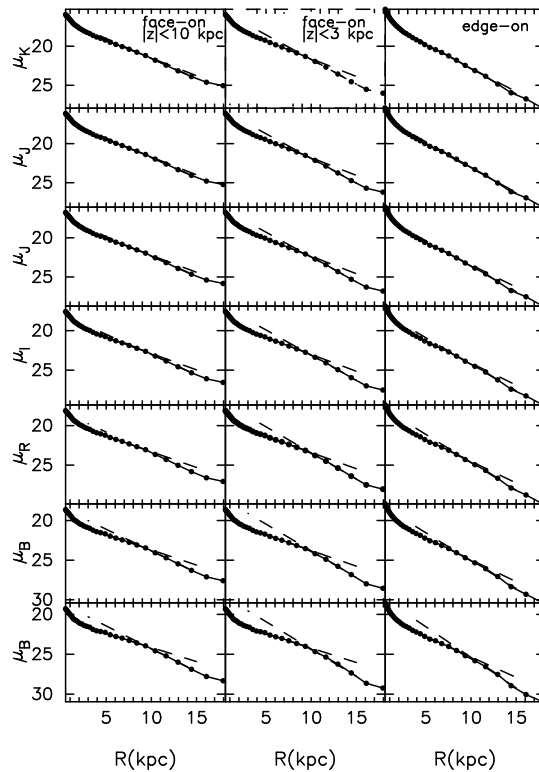


**Figure A1.** Surface brightness profiles in different bands calculated in face-on (azimuthally averaging) and edge-on configurations. For the face-on projection we have integrated between different distances from the disc mid-plane, as indicated in the inset.

position of the break and the angle between the two exponential fits in each configuration.

We do not find any fundamental difference between the position of the break or its intensity for the face-on and edge-on values; they agree, within the uncertainties. The table also shows the measured inner and outer scale-lengths. The uncertainties in the measurement of the scale-length are  $<0.1\%$  and are, therefore, not listed. We can see that contrary to what happens with the position of the break, we did find differences in the scale-lengths of the disc when measured at different inclinations. In particular, the scale-lengths are systematically lower in the edge-on projections, counter to that claimed by van der Kruit (2008). Due to the smaller scale-length obtained in edge-on systems, the  $R_{\text{BR}}/h$  measured for this projection is larger than for the face-on projection. These differences have been found previously in empirical studies, but it is not clear if they are due to projection effects or to different techniques to mark the break (see Trujillo & Pohlen 2006).

Finally, we do not find a sharper edge in edge-on galaxies than for face-on systems, for which we conclude that this effect, reported in observations, must be the consequence of dust extinction.

	band	face-on $ z  < 10$ kpc	face-on $ z  < 3$ kpc	edge-on
R <sub>br</sub>	B	$9.3 \pm 0.3$	$9.6 \pm 0.7$	$9.8 \pm 1.0$
h <sub>inn</sub>	B	2.83	2.75	1.95
h <sub>out</sub>	B	1.74	1.46	1.30
angle	B	10.2	14.4	10.4
R <sub>br</sub>	V	$9.2 \pm 0.4$	$9.5 \pm 0.6$	$9.3 \pm 1.3$
h <sub>inn</sub>	V	2.61	2.53	1.81
h <sub>out</sub>	V	1.83	1.47	1.41
angle	V	7.6	12.5	6.3
R <sub>br</sub>	R	$8.9 \pm 0.7$	$9.8 \pm 0.4$	$9.2 \pm 1.7$
angle	R	5.9	11.1	6.5
h <sub>inn</sub>	R	2.51	2.43	1.83
h <sub>out</sub>	R	1.90	1.52	1.42
R <sub>br</sub>	I	$8.7 \pm 1.1$	$9.6 \pm 0.4$	$8.3 \pm 1.0$
angle	I	4.6	9.3	4.2
h <sub>inn</sub>	I	2.42	2.34	1.80
h <sub>out</sub>	I	1.96	1.57	1.52
R <sub>br</sub>	J	$8.2 \pm 1.7$	$9.5 \pm 0.3$	$7.8 \pm 1.4$
angle	J	3.4	8.2	3.4
h <sub>inn</sub>	J	2.31	2.24	1.76
h <sub>out</sub>	J	1.99	1.58	1.54
R <sub>br</sub>	H	$8.1 \pm 2.9$	$9.5 \pm 0.3$	$12.1 \pm 6.0$
h <sub>inn</sub>	H	2.20	2.20	1.60
h <sub>out</sub>	H	2.00	1.59	1.52
angle	H	2.1	7.7	1.3
R <sub>br</sub>	K	$9.2 \pm 2.1$	$9.4 \pm 0.3$	–
h <sub>inn</sub>	K	2.22	2.19	1.65
h <sub>out</sub>	K	1.95	1.58	1.55
angle	K	2.8	7.7	0

**Table A1.** Break radius and angle between the two exponential fits in different bands.